www.czasopisma.pan.pl PAN POLSKA AKADEMIA NAUK www.journals.pan.pl

ARCHIVES OF ACOUSTICS
36, 1, 121–139 (2011)

DOI: 10.2478/v10168-011-0009-9

Acoustic Pressure Radiated by a Circular Membrane Into the Quarter-Space

Wojciech P. RDZANEK[(1)], Krzysztof SZEMELA[(1)], Dawid PIECZONKA[(2)]

[(1)] *University of Rzeszów*
Department of Acoustics, Institute of Physics
Al. Rejtana 16A, 35-310 Rzeszów, Poland
e-mail: wprdzank@univ.rzeszow.pl

[(2)] *Stylem*
Trzebownisko 614, 36-001 Trzebownisko, Poland

(*received May 29, 2009; accepted January 13, 2011*)

The Neumann boundary value problem for the Helmholtz equation within the quarter-space has been considered in this paper. The Green function has been used to find the acoustic pressure amplitude as the approximation valid within the Fraunhoffer's zone for some time-harmonic steady state processes. The low fluid loading has been assumed and the acoustic attenuation has been neglected. It has also been assumed that the vibration velocity of the acoustic particles is small as compared with the sound velocity in the gaseous medium.

Keywords: acoustic pressure, Fraunhoffer's zone, Green function, circular membrane.

1. Introduction

Some vibrating flat surface elements mounted in the vicinity of some flat vertical walls often become sound sources. There are many vertical walls of residential buildings, shopping malls, supermarkets and office buildings in urban environments. Such walls reflect sound waves and modify considerably the acoustic field generated if the sizes of the walls are large compared to the lengths of acoustic waves. Therefore, the theoretical prediction of acoustic field near the walls of large size is useful modelling the acoustic climate of urban and industrial environments where the sound field can not be treated as a free field. The acoustic waves are radiated into the semi-free region that is partially bounded by the walls. The measurements of some acoustic quantities such as the amplitude of the acoustic pressure, the space distribution of the acoustic pressure level, the acoustic power and the acoustic impedance of the acoustic radiators mounted in the vicinity of the

walls being high as compared with the sizes of the radiators as well as compared to the radiated wavelengths become significant from the practical view-point. The former two quantities are equivalent to one another whereas one of the latter is necessary to include the acoustic attenuation in the theoretical predictions of acoustic pressure level. The results obtained are useful for both planning the urban areas and minimizing vibrations and generated noise (Dykas *et al.*, 2010; Gołaś, Filipek, 2009; Gołaś *et al.*, 2010; Piddubniak, Piddubniak, 2010; Walerian *et al.*, 2010a,b; Weyna, 2010). The piezoelectric effect is widely used for this purpose within the low frequency range (Batko, Kozupa, 2008; Kozień, Wiciak, 2009; Kozupa, Wiciak, 2010; Le Clézio *et al.*, 2008; Leniowska, 2008, 2009; Pawełczyk, 2008; Zou, Crocker, 2009b). On the other hand, the predictions of space distributions of acoustic pressure and acoustic power are difficult or impossible until the walls are built in a given configuration. The influence of the changes in the configuration of the walls on the acoustic pressure distribution is also difficult to predict. In this case, some elementary theoretical formulations of the acoustic quantities mentioned above can be useful for some flat elements vibrating and radiating the acoustic waves. The elementary approximate formulas are derived using simplifying assumptions. Nevertheless, they are convenient for initial estimations of the acoustic pressure distribution at the design stage of some configurations of the vertical walls.

So far, theoretical expressions have been derived and measurements have been conducted for the acoustic impedance and for the acoustic pressure for the simplest piston radiators of the circular and rectangular geometry that have been embedded on the flat baffles (Arase, 1964; Greenspan, 1979; Rdzanek, Szemela, 2007; Rdzanek *et al.*, 2007; Stepanishen, 1974; Svensson, 2001; Thompson, 1971). The distribution of the acoustic pressure and the acoustic pressure level of some simplest deformable acoustic sources such as vibrating circular plates and membranes embedded onto a flat baffle have been investigated theoretically or measured and all has been reported e.g. by Cieślik and Pieczara (2008); Krishnappa and McDougall (1989); Rdzanek (1990); Shuyu (2000). The acoustic power and the acoustic impedance of such sources have been presented by Lee and Singh (2005); Levine and Leppington (1988); Stepanishen and Ebenezer (1992); Zou and Crocker (2009a).

Few papers deal with the sound radiation within the region of the quarter-space. The acoustic radiation of the vibrating sphere in the vicinity of the quarter-space has been described in detail by Hasheminejad and Azarpeyvand (2004). The acoustic power radiated into the quarter-space by a vibrating circular membrane has been presented by Rdzanek, Rdzanek, and Szemela (2009). The distribution of the acoustic pressure radiated into the quarter-space and into the semi-quarter-space by a vibrating circular piston has been presented by Rdzanek, Szemela, and Pieczonka (2007). The acoustic pressure has been formulated as an approximation valid for the Franhoffer's zone. So far such approximations have not been presented for a vibrating circular membrane. Ob-

viously, a deformable membrane is a better model of a real vibrating surface radiator than a rigid piston. Therefore, the problem of sound radiation by a vibrating circular membrane embedded onto one of the two baffles perpendicular to one another and bounding the quarter-space has been considered in this paper. It has been assumed that the influence of the acoustic attenuation on the membranes' vibrations is small enough in the air to be neglected for frequencies different from the membrane's eigenfrequencies. The acoustic pressure radiated into the quarter-space has been investigated for two different surface excitation of the membrane. The Green function presented by RDZANEK and RDZANEK (2006) has been used as the basis of solution. The approximation used has made it possible to express the acoustic pressure distribution at the Fraunhoffer's zone using some elementary functions.

2. The analysis assumptions

A circular membrane of radius a is embedded onto one of the two flat perfectly rigid baffles, perpendicular to one another, for $z = 0$. The membrane's centre is indicated by the leading vector $\mathbf{l} = (0, l, 0)$ (cf. Fig. 1) and its surface is excited by an asymmetric external pressure. It has been assumed that the acoustic particles adjacent directly to the membrane's surface vibrate as acoustic monopoles with the amplitude equal to the normal component value of the membrane's vibration vector. The backward interactions of the air column vibrations on the membrane's motion have been neglected. The time-harmonic steady state processes have been analysed varying with respect to time according to $\exp(-i\omega t)$ where ω is the excitation circular frequency.

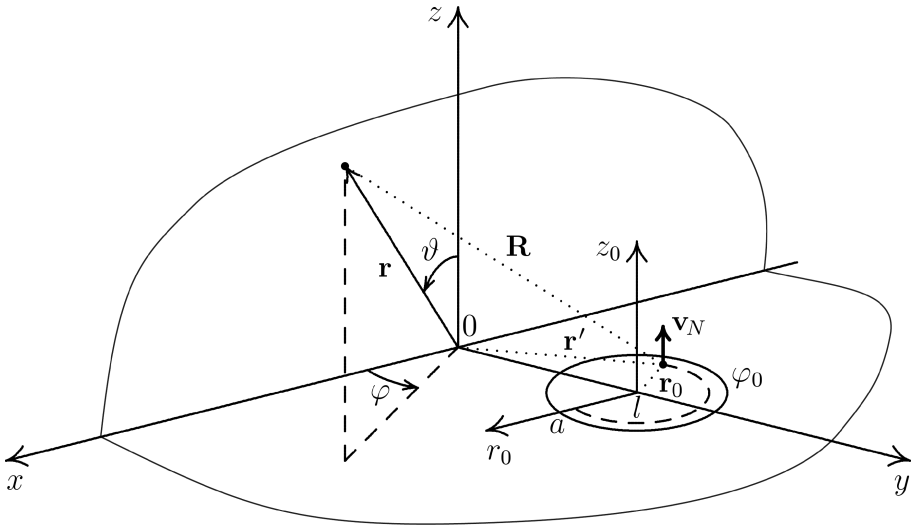

Fig. 1. The circular membrane's location within the quarter-space region Ω for $z = 0$ where $\mathbf{r}_0 = \mathbf{r}' - \mathbf{l}$ and $\mathbf{R} = \mathbf{r} - \mathbf{r}'$.

The main aim of this study is to determine the acoustic pressure distribution within the region Ω bounded by the baffles at a big distance from the radiator as compared with the radiator's geometric sizes. The Cartesian coordinates have been used to describe the generated acoustic waves. The quarter-space region has been defined as $\Omega = \{-\infty < x < \infty,\ 0 \leq y < \infty,\ 0 \leq z < \infty\}$. The vector $\mathbf{r}$ indicates the location of the acoustic field's point, the vector $\mathbf{r}'$ indicates the source's point using the global coordinates and the vector $\mathbf{r}_0$ indicates the same point using the local coordinates with the origin indicated by the vector $\mathbf{l}$ (Fig. 1). The equation of motion of the excited circular membrane using the local polar coordinates assumes the form of

$$\left(k_T^{-2}\nabla^2 + 1\right) W(r_0, \varphi_0) = -\frac{f(r_0, \varphi_0)}{\omega^2 \sigma}, \tag{1}$$

where ω and σ are the vibration circular frequency and the surface density of the membrane, respectively, $k_T = \omega / c_M$ is the structural wavenumber, $c_M = \sqrt{T/\sigma}$ is the propagation velocity of the wave propagated on the membrane's surface, T is the membrane's stretching force related to its circumference length unit, $f(r_0, \varphi_0)$ is the external excitation distribution on the membrane's surface. The solution represents the membrane's transverse deflection amplitude and has been formulated as the complete eigenfunction series

$$W(r_0, \varphi_0) = \sum_{m=0}^{\infty} \sum_{n=1}^{\infty} \left\{ c_{mn}^{(c)} W_{mn}^{(c)}(r_0, \varphi_0) + c_{mn}^{(s)} W_{mn}^{(s)}(r_0, \varphi_0) \right\}, \tag{2}$$

where $W_{mn}^{(c)}(r_0, \varphi_0)$ and $W_{mn}^{(s)}(r_0, \varphi_0)$ are the eigenfunctions (cf. MEIROVITCH (1967)). The eigenfunctions are also the solutions of the equation of motion

$$\left(\nabla^2 + k_{mn}^2\right) \left\{ \begin{array}{c} W_{mn}^{(c)}(r_0, \varphi_0) \\ W_{mn}^{(s)}(r_0, \varphi_0) \end{array} \right\} = 0 \tag{3}$$

for the free vibrations for the mode (m, n). The solutions are degenerated to the two eigenfunctions for one mode, i.e. cosine and sine, for $m \geq 1$. The membrane's transverse deflection W has been been defined herein as the function of the spatial variables r and φ with the index 0 to emphasize the fact that this quantity is defined in the local polar coordinates which is helpful for further analysis.

The eigenfunctions, expressed in these local coordinates, assume therefore the form of

$$\begin{gathered} \left\{ \begin{array}{c} W_{mn}^{(c)}(r_0, \varphi_0) \\ W_{mn}^{(s)}(r_0, \varphi_0) \end{array} \right\} = W_{mn}(r_0) \left\{ \begin{array}{c} \cos m\varphi_0 \\ \sin m\varphi_0 \end{array} \right\}, \\ W_{mn}(r_0) = \sqrt{\varepsilon_m}\, \frac{J_m(k_{mn} r_0)}{J_{m+1}(\beta_{mn})}, \end{gathered} \tag{4}$$

where $\lambda_{mn} = k_{mn} a$ is the eigenvalue satisfying the membrane's frequency equation $J_m(\lambda_{mn}) = 0$, $k_{mn} = \omega_{mn} / c_M$, ω_{mn} is the eigenfrequency of the mode (m, n),

$\varepsilon_0 = 1$ and $\varepsilon_m = 2$ for $m \geq 1$. The eigenfunctions' orthogonality condition assumes the form of

$$\frac{1}{S_0}\int_{S_0}\left\{\begin{array}{c} W_{mn}^{(c)}(r_0,\varphi_0) \\ W_{mn}^{(s)}(r_0,\varphi_0) \end{array}\right\}\left\{\begin{array}{c} W_{m'n'}^{(c)}(r_0,\varphi_0) \\ W_{m'n'}^{(s)}(r_0,\varphi_0) \end{array}\right\} \mathrm{d}S_0 = \delta_{mm'}\delta_{nn'}, \tag{5}$$

where $\delta_{mm'}$ is the Kronecker delta, $S_0 = \pi a^2$ and $\mathrm{d}S_0 = r_0\, dr_0\, d\varphi_0$. Inserting the solution (2) to Eq. (1) yields

$$\left\{\begin{array}{c} c_{mn}^{(c)} \\ c_{mn}^{(s)} \end{array}\right\} = \frac{1}{\omega^2\sigma\left(k_T^{-2}k_{mn}^2 - 1\right)}\left\{\begin{array}{c} f_{mn}^{(c)} \\ f_{mn}^{(s)} \end{array}\right\} \tag{6}$$

after using Eq. (3), where

$$\left\{\begin{array}{c} f_{mn}^{(c)} \\ f_{mn}^{(s)} \end{array}\right\} = \frac{1}{S_0}\int_{S_0}\left\{\begin{array}{c} W_{mn}^{(c)}(r_0,\varphi_0) \\ W_{mn}^{(s)}(r_0,\varphi_0) \end{array}\right\} f(r_0,\varphi_0)\ \mathrm{d}S_0. \tag{7}$$

The expression (6) enables to determine the coupling matrix coefficients $c_{mn}^{(c)}$ and $c_{mn}^{(s)}$ appearing in the solution (2) for a given surface excitation. The acoustic attenuation has been neglected in any further computations presented in this paper. However it can be included by using the values of the acoustic impedance presented by Rdzanek, Rdzanek, and Szemela (2009).

3. Sound pressure amplitude

The amplitude of the acoustic pressure radiated by the excited membrane for harmonic steady state vibrations of the acoustic particles can be formulated as

$$p(\mathbf{r}) = -ik\varrho_0 c\int_{S'} v_N(\mathbf{r}')\, G(\mathbf{r}\,|\,\mathbf{r}')\ \mathrm{d}S' \tag{8}$$

on the basis of the sharpened Sommerfeld radiation condition (Rubinowicz, 1971) and on the basis of the Neumann boundary conditions satisfied on the surface of the rigid baffles where k is the acoustic wavenumber, ϱ_0 and c are the air column density and the sound velocity in the air, respectively, $v_N(\mathbf{r}_0)$ is the normal component of the vibration velocity amplitude of the membrane, $G(\mathbf{r}\,|\,\mathbf{r}')$ is the Green function and $S' \equiv S_0$ is the area directly adjacent to the vibrating membrane's surface. It can be assumed that the normal component of the membrane's vibration velocity amplitude $v_N(\mathbf{r}')$ is approximately equal to the vibration velocity amplitude of the acoustic particle directly adjacent to the membrane for the small vibration velocity as compared with the sound velocity in the air.

The membrane's vibration velocity has been formulated as the following eigenfunction series (cf. MEIROVITCH 1967; RDZANEK *et al.*, 2009)

$$v_N(r_0,\varphi_0) = -i\omega W(r_0,\varphi_0) = \sum_{m=0}^{\infty}\sum_{n=1}^{\infty}\frac{\omega}{\omega_{mn}}\left\{c_{mn}^{(c)}v_{mn}^{(c)}(r_0,\varphi_0)+c_{mn}^{(s)}v_{mn}^{(s)}(r_0,\varphi_0)\right\}, \tag{9}_1$$

$$\left\{\begin{array}{c} v_{mn}^{(c)}(r_0,\varphi_0) \\ v_{mn}^{(s)}(r_0,\varphi_0)\end{array}\right\} = v_{mn}(r_0)\left\{\begin{array}{c}\cos m\varphi_0 \\ \sin m\varphi_0\end{array}\right\}, \qquad v_{mn}(r_0) = -i\omega_{mn}W_{mn}(r_0), \tag{9}_2$$

where the mode (m,n) degenerates to the cosine and sine modeshapes $v_{mn}^{(c)}(r_0,\varphi_0)$ and $v_{mn}^{(s)}(r_0,\varphi_0)$ (modal vibration velocities of the membrane) for $m \geq 1$. The vibrating membrane's transverse deflection amplitude can be formulated as

$$W(r_0,\varphi_0) = \sum_{m=0}^{\infty}\sum_{n=1}^{\infty}\left\{c_{mn}^{(c)}W_{mn}^{(c)}(r_0,\varphi_0)+c_{mn}^{(s)}W_{mn}^{(s)}(r_0,\varphi_0)\right\}. \tag{10}$$

The Green function for the considered boundary value problem has been expressed as

$$G(\mathbf{r}\,|\,\mathbf{r}_0) = \frac{\exp(ikR_l)}{2\pi R_l} + \frac{\exp(ikR_{-l})}{2\pi R_{-l}} \tag{11}$$

for $z' = 0$ using the Weyl equation (WEYL, 1919) where $R_l \equiv |\mathbf{R}_l| = |\mathbf{r}-\mathbf{r}'| = \{(x-x')^2+(y-y')^2+z^2\}^{1/2}$ is the distance between the acoustic particle directly adjacent to the vibrating membrane and the acoustic field's point, l is the y coordinate of the vector $\mathbf{l}$ and also is the distance between the membrane's center or the center of the membrane's image and the vertical baffle in the global Cartesian coordinates. The resultant Green function is the superposition of the two terms. The distance is equal to l for the membrane and is equal to $-l$ for its image. It is worth noticing that the Green function formulated as above can also be obtained using the method of images. Consequently, it has been obtained that

$$p(\mathbf{r}) = \sum_{m=0}^{\infty}\sum_{n=1}^{\infty}\frac{\omega}{\omega_{mn}}\left\{c_{mn}^{(c)}p_{mn}^{(c)}(\mathbf{r})+c_{mn}^{(s)}p_{mn}^{(s)}(\mathbf{r})\right\} \tag{12}$$

after inserting the series from Eq. (9)1 into Eq. (8) where sign_m is the signum function and

$$\left\{\begin{array}{c} p_{mn}^{(c)}(\mathbf{r}) \\ p_{mn}^{(s)}(\mathbf{r})\end{array}\right\} = -ik\varrho_0 c\int_{S'}\left\{\begin{array}{c} v_{mn}^{(c)}(\mathbf{r}') \\ v_{mn}^{(s)}(\mathbf{r}')\end{array}\right\} G(\mathbf{r}\,|\,\mathbf{r}')\,\mathrm{d}S'. \tag{13}$$

The cosine and sine modal sound pressure amplitudes appearing in Eqs. (12) and (13) result from the asymmetric mode degeneration indicated in Eq. (9). Further the following transformations have been introduced from the global Carte-

sian coordinates to the global spherical coordinates and to the local polar coordinates

$$x = r\sin\vartheta\cos\varphi, \qquad y = r\sin\vartheta\sin\varphi, \qquad z = r\cos\vartheta, \tag{14}_1$$

$$x' = r_0\cos\varphi_0, \qquad y' = l + r_0\sin\varphi_0. \tag{14}_2$$

The distance R_l has been formulated as the expansion series around the point $r_0/r = 0$ assuming that $r \gg r_0$ which has yielded the distance approximation

$$R_l \approx Q_l + r_0\left(\alpha_l\cos\varphi_0 + \beta_l\sin\varphi_0\right) + O(r_0^2/r^2), \tag{15}$$

where the distance between the membranes center $(0, l, 0)$ and the observation point (r, ϑ, φ) has been denoted as

$$Q_l = \left(l^2 + r^2 - 2rl\sin\vartheta\sin\varphi\right)^{1/2} \tag{16}_1$$

and

$$\alpha_l = -r\sin\vartheta\cos\varphi/Q_l, \qquad \beta_l = \left(|l| - r\sin\vartheta\sin\varphi\,\mathrm{sign}l\right)/Q_l. \tag{16}_2$$

The assumption $r \gg r_0$ means that the above approximation is valid in the far field. The following approximation has been used

$$\frac{\exp(ikR_l)}{2\pi R_l} \approx \frac{\exp(ikQ_l)}{2\pi Q_l}\,\exp\{ikr_0\left(\alpha_l\cos\varphi_0 + \beta_l\sin\varphi_0\right)\} \tag{17}$$

given that the numerator in Eq. (11) grows rapidly with an increase in R_l and given that the denominator is slowly varying with changes of R_l. It has been inserted into Eq. (11) and further into Eq. (13) yielding

$$\begin{Bmatrix} p_{mn}^{(c)}(\mathbf{r}) \\ p_{mn}^{(s)}(\mathbf{r}) \end{Bmatrix} = -\frac{ik\varrho_0 cS_0}{2\pi} \cdot \left(\frac{\exp(ikQ_l)}{Q_l}\begin{Bmatrix} M_{l,mn}^{(c)}(\mathbf{r}) \\ M_{l,mn}^{(s)}(\mathbf{r}) \end{Bmatrix} + \frac{\exp(ikQ_{-l})}{Q_{-l}}\begin{Bmatrix} M_{-l,mn}^{(c)}(\mathbf{r}) \\ M_{-l,mn}^{(s)}(\mathbf{r}) \end{Bmatrix}\right), \tag{18}$$

where

$$\begin{Bmatrix} M_{l,mn}^{(c)}(\mathbf{r}) \\ M_{l,mn}^{(s)}(\mathbf{r}) \end{Bmatrix} = \frac{1}{S_0}\int\limits_{S_0}\begin{Bmatrix} v_{mn}^{(c)}(\mathbf{r}_0) \\ v_{mn}^{(s)}(\mathbf{r}_0) \end{Bmatrix}\exp\{ikr_0\left(\alpha_l\cos\varphi_0 + \beta_l\sin\varphi_0\right\}\,\mathrm{d}S_0$$

$$= \frac{2}{a^2}\int\limits_0^a v_{mn}(r_0)\begin{Bmatrix} F_{l,m}^{(c)}(r_0) \\ F_{l,m}^{(s)}(r_0) \end{Bmatrix} r_0\,\mathrm{d}r_0, \tag{19}_1$$

$$\begin{Bmatrix} F_{l,m}^{(c)}(r_0) \\ F_{l,m}^{(s)}(r_0) \end{Bmatrix} = \frac{1}{2\pi}\int\limits_0^{2\pi}\exp\{ikr_0\left(\alpha_l\cos\varphi_0 + \beta_l\sin\varphi_0\right)\}\begin{Bmatrix} \cos m\varphi_0 \\ \sin m\varphi_0 \end{Bmatrix}\mathrm{d}\varphi_0$$

$$= i^m J_m(\gamma_l r_0)\begin{Bmatrix} \cos m\varphi \\ \sin m\varphi \end{Bmatrix} \tag{19}_2$$

and $\gamma_l = k\left(\alpha_l^2 + \beta_l^2\right)^{1/2}$. The modal quantities $M_{l,mn}^{(c)}(\mathbf{r})$ and $M_{l,mn}^{(s)}(\mathbf{r})$ from Eq. $(19)_1$ describe the sound radiation related to the vibration mode (m,n). It has been obtained

$$\left\{ \begin{array}{c} M_{l,mn}^{(c)}(\mathbf{r}) \\ M_{l,mn}^{(s)}(\mathbf{r}) \end{array} \right\} = -i^{m+1}\omega_{mn}\sqrt{\varepsilon_m}\,\psi_{l,\,mn} \left\{ \begin{array}{c} \cos m\varphi \\ \sin m\varphi \end{array} \right\} \tag{20}$$

after integrating over the variable r_0 in Eq. $(19)_1$ where

$$\psi_{l,\,mn} = \frac{2}{a^2}\int_0^a \frac{J_m(k_{mn}r_0)}{J_{m+1}(\lambda_{mn})}\,J_m(\gamma_l r_0)\,r_0\,\mathrm{d}r_0 = \frac{2\lambda_{mn}J_m(\gamma_l a)}{\lambda_{mn}^2 - (\gamma_l a)^2}. \tag{21}$$

Equation (20) has been inserted into Eq. (18) giving the acoustic pressure

$$p(\mathbf{r}) = p_l(\mathbf{r}) + p_{-l}(\mathbf{r}) \tag{$22)_1$}$$

formulated as the superposition of the pressure amplitudes generated by the original source $p_l(\mathbf{r})$ and by its image $p_{-l}(\mathbf{r})$ where it has been denoted that

$$p_l(\mathbf{r}) = -\frac{kS_0}{2\pi}\,\varrho_0 c\omega\,\frac{e^{ikQ_l}}{Q_l}\sum_{m=0}^{\infty}\sum_{n=1}^{\infty} i^m\sqrt{\varepsilon_m}\,\psi_{l,\,mn} \cdot \left\{c_{mn}^{(c)}\cos m\varphi + c_{mn}^{(s)}\sin m\varphi\right\}. \tag{$22)_2$}$$

These equations represent the approximation of the acoustic pressure amplitude valid in a big distance between the observation point and the vibrating membrane as compared with the membrane's geometric sizes.

4. Numerical analysis

4.1. Forced vibrations

The following two surface excitations of the membrane have been used for the numerical computations (cf. Rdzanek *et al.*, 2009)

$$f_1(r_0,\varphi_0) = f_1\,\frac{S}{r}\,\delta(r_0 - \overline{r}_0)\,\delta(\varphi_0 - \overline{\varphi}_0), \tag{$23)_1$}$$

$$f_2(r_0,\varphi_0) = f_2 \left\{ \begin{array}{ll} 1; & 0 \leqslant r_0 \leqslant b \\ 0; & b < r_0 \leqslant a \end{array} \right\} (\cos M\varphi_0 - \overline{\varphi}_0) \tag{$23)_2$}$$

for $0 \leqslant b \leqslant a$, where f_1 and f_2 [Pa] are the excitation amplitudes. The first excitation is the concentrated force f_1 exerted to the membrane at the point $(\overline{r}_0, \overline{\varphi}_0)$ and described by the Dirac delta function. This theoretical model of excitation is useful for integration. However, it is necessary to remember that the real membrane must be excited by the force exerted to a finite part of its

surface to avoid damage. This excitation will be briefly referred to as the Dirac excitation. The second excitation is described by the cosine function. It means that the distribution of the excitation is uniform with respect to the local radial variable r_0 and varies cosinusoidally with respect to the local angle variable φ_0 and assumes its maximum for $\varphi_0 = \overline{\varphi}_0$. The M full variation periods are covered within the limits $(0, 2\pi)$ and the excitation shows M node lines. Consequently, the modes contribute the membrane's response only for $m = M$. The response has the node point for $r_0 = 0$ and $M \geq 1$ (cf. Eq. (4)) and is much weaker than the response for the Dirac excitation. Therefore, the amplitudes of f_2 must be assumed to be considerably higher than f_1 to obtain comparable amplitudes of the transverse deflection amplitude. This excitation will be briefly referred to as the cosine excitation. The membrane's response is essentially asymmetric except of the two cases. One case is when $\overline{r}_0 = 0$ for the Dirac excitation and the second is when $M = 0$ for the cosine excitation. Obviously, a number of excitations can be modelled but the two presented have been arbitrarily selected as the most representative for asymmetric vibrations and sound pressure distributions.

The following values of the modal excitation coefficients have been obtained by inserting Eqs. (23) into (7)

$$\begin{Bmatrix} f^{(c)}_{1,mn} \\ f^{(s)}_{1,mn} \end{Bmatrix} = f_1 \begin{Bmatrix} W^{(c)}_{mn}(\overline{r}_0, \overline{\varphi}_0) \\ W^{(s)}_{mn}(\overline{r}_0, \overline{\varphi}_0) \end{Bmatrix}, \tag{24}_1$$

$$\begin{Bmatrix} f^{(c)}_{2,mn} \\ f^{(s)}_{2,mn} \end{Bmatrix} = f_2 \frac{\delta_{mM}}{\epsilon_m} \overline{F}_{mn}(b) \begin{Bmatrix} \cos\overline{\varphi}_0 \\ \sin\overline{\varphi}_0 \end{Bmatrix}, \tag{24}_2$$

where

$$\overline{F}_{mn}(b) = \frac{2}{a^2} \int_0^b W_{mn}(r)\, r \, \mathrm{d}r. \tag{25}$$

First, the amplitude of the membrane's transverse deflection has been calculated for the two surface excitations defined in Eqs. (23) to help further reading the corresponding distributions of the resultant acoustic pressure amplitudes. Performing the numerical calculations requires assuming the complete set of the physical properties of the membrane, its surrounding gaseous medium, the considered region Ω and the excitation. The following properties have been arbitrarily selected:

$$\begin{aligned} a &= 0.2 \text{ m}, & \sigma &= 0.5 \text{ kg/m}^2, & T &= 500 \text{ N/m}, \\ l &= 1.0 \text{ m}, & c &= 343 \text{ m/s}, & \varrho_0 &= 1.23 \text{ kg/m}^3, \\ f_1 &= 1 \text{ Pa}, & f_2 &= 1 \text{ kPa}, & \overline{r}_0 &= 0.1 \text{ m}, \\ \overline{\varphi}_0 &= \pi/4, & b &= 0.1 \text{ m}, & f &= 500 \text{ Hz}. \end{aligned}$$

They result in the certain set of the membrane's eigenfrequencies. The lowest of them have been collected in Table. 1. If any of these parameters have been modified it has been mentioned in the corresponding figure captions.

Table 1. The lowest eigenfrequencies $f_{m,n}$ [Hz] of the circular membrane for the modes (m,n) used in the numerical computations.

m	n							
	1	2	3	4	5	6	7	8
0	60.52	138.91	217.77	296.73	375.73	454.75	533.78	612.82
1	96.42	176.54	256.01	335.29	414.48	493.63	572.75	651.86
2	129.24	211.82	292.41	372.34	451.95	531.40	610.75	690.03
3	160.55	245.63	327.52	408.26	488.43	568.29	647.94	727.47
4	190.96	278.44	361.68	443.30	524.10	604.43	684.45	764.27
5	220.73	310.50	395.09	477.63	559.10	639.95	720.38	800.53
6	250.04	341.97	427.89	511.37	593.54	674.92	755.79	836.30
7	278.98	372.97	460.20	544.60	627.48	709.42	790.74	871.63

The resultant membrane's vibration profiles are shown in Fig. 2. They represent the membrane's response for the given excitations and can be useful for understanding some further distributions of the corresponding acoustic pressure amplitudes in the far field. The first row of this figure shows the complex distributions of the profiles which is caused, obviously, by the superposition of a number of the lowest membrane's modes that dominantly contribute them. The second row shows their intersections for $\varphi_0 = \overline{\varphi}_0 = \pi/4$ and the third row illustrates the corresponding approximation error. Figure 2a shows the membrane's response for the Dirac excitation. The point where excitation is exerted is invisible on the perspective view. However, it can easily be noted on the intersection for $r_0 = 0.1$. Paradoxically, the membrane's response at this point is small as compared with the rest of the intersection but the response of its close neighbourhood assumes significant values about minus unity. This is the consequence of the complex superposition of the contributing modes and this can vary considerably with the change in the excitation frequency f. It is worth noticing for this kind of excitation that all the modes of the membrane are excited except of the modes having the node at the point where the excitation is exerted. However, only some of the modes contributes the output dominantly. Figure 2b shows the membrane's response for the cosine excitation. It can be noted that for the selected excitation frequency only a part of the membrane's area located around its centre responses considerably on the cosine excitation. This is the consequence of the nature of this excitation which excites only the selected modes for $m = M$. Also a nodal point at $r_0 = 0$ can be observed. It is the intersection of the nodal lines of the excited modes.

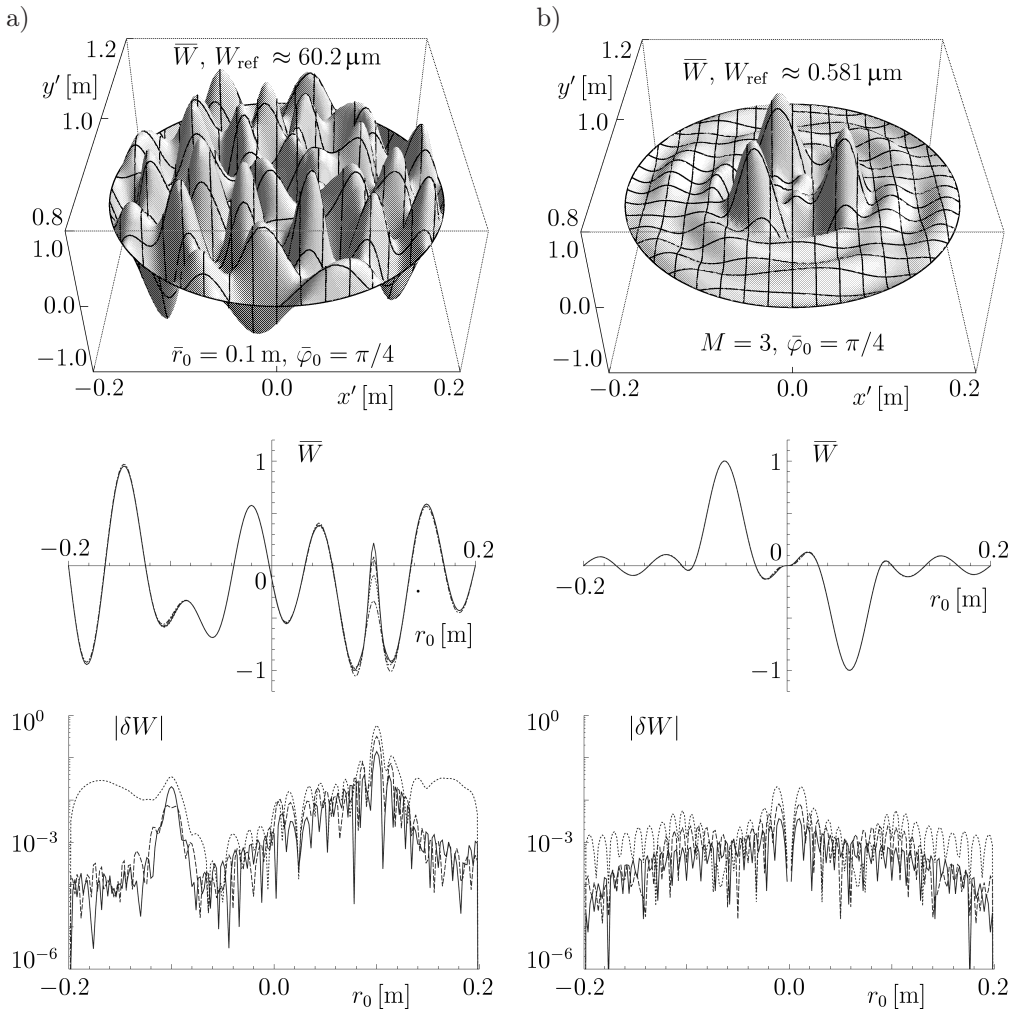

Fig. 2. The normalized membrane's transverse deflection amplitude $\overline{W}$ and its relative error estimation δW for: a) the Dirac excitation; b) the cosine excitation. Key for the intersections of $\overline{W}$: —— $N = 30$, – – – $N = 25$, ····· $N = 20$, –·–· $N = 15$. Key for the error estimations $|\delta W|$: —— $N = 25$, – – – $N = 20$, ····· $N = 15$.

The question arises what is the approximation error resulting from the truncation in the eigenfunction series given in Eq. (9) and to what number of the lowest modes it should be limited? It has been found that for the selected properties of the radiator and its surroundings the reference value of W_{ref} can be achieved by assuming the maximum modenumbers $m-1, n = 30$ which is enough to test the computation accuracy of the normalized membrane's transverse deflection amplitude defined as

$$\overline{W} = \frac{W}{W_{\mathrm{ref}}}, \qquad W_{\mathrm{ref}} = \max_{r_0,\varphi_0} |W|. \tag{26}$$

The approximation error has been defined as

$$\delta W = \frac{W_N - W_{N=30}}{\max_{r_0,\varphi_0} |W_{N=30}|}, \tag{27}$$

where the index N denotes the number of terms used in the eigenfunction series (10).

The membrane's profile intersections for $\overline{W}$ shown in the second row in Fig. 2 present four curves for the Dirac excitation and four curves for the cosine excitation for the following maximum values of the modal number $N = \max\{m-1, n\} = 30$ (solid lines), 25 (dashed lines), 20 (dotted lines) and 15 (dashed-dotted lines). It is difficult to distinguish the lines except of the close neighbourhood of the concentrated force exertion point for the Dirac excitation. This means that even using the matrix of 15×15 modes gives, i.e. for $N = 15$, a good approximation of the profiles beyond the mentioned above exception. This exception however should not cause any significant problem while calculating the resultant acoustic pressure amplitude since it is essentially the integral quantity, i.e. it is the sum of all the infinitesimal contributions from the acoustic particles adjacent directly to the surface of vibrating membrane (cf. Eq. (13)). This hypothesis will be tested numerically later. The error estimation caused by truncation has been illustrated in the third row in Fig. 2. It has been shown that the matrix of $N = 15$ is enough to assure that the error is smaller than 10% beyond the mentioned exception for the Dirac excitation (cf. the dotted lines for $N = 15$). The higher accuracy requires increasing the maximum number N – see the remaining curves for $N = 20$ – the dashed lines and for $N = 25$ – the solid lines. It can be noted that $N = 20$ is enough to assure that the approximation error is considerably smaller than 1‰ except small areas around the exertion point for the Dirac excitation (where exceptionally even $N = 30$ is not enough) and that $N = 15$ is enough to achieve the error level about 1‰ for the cosine excitation except the small area at the membrane's centre.

4.2. Acoustic pressure

All the graphs in Figs. 3–5 have been prepared for a big distance from the corner of the region Ω (from the origin of the coordinates system) for $r \equiv |\mathbf{r}| = 100$ m assuming that the membrane is excited by the time-harmonic surface pressure at the frequency $f = 500$ Hz. Only Fig. 5b has been prepared for $r = 2.5$ [m]. The matrix of the 25^2 initial modes of the membrane has been used for the numerical computations, i.e. the modenumbers $m = 0, \ldots, 24$ and $n = 1, \ldots, 25$ to assure high accuracy. All the remaining parameter values have been assumed identically as in Subsec. 4.1 unless stated differently in the figure captions. The initial eigenfrequencies have been taken from Table 1.

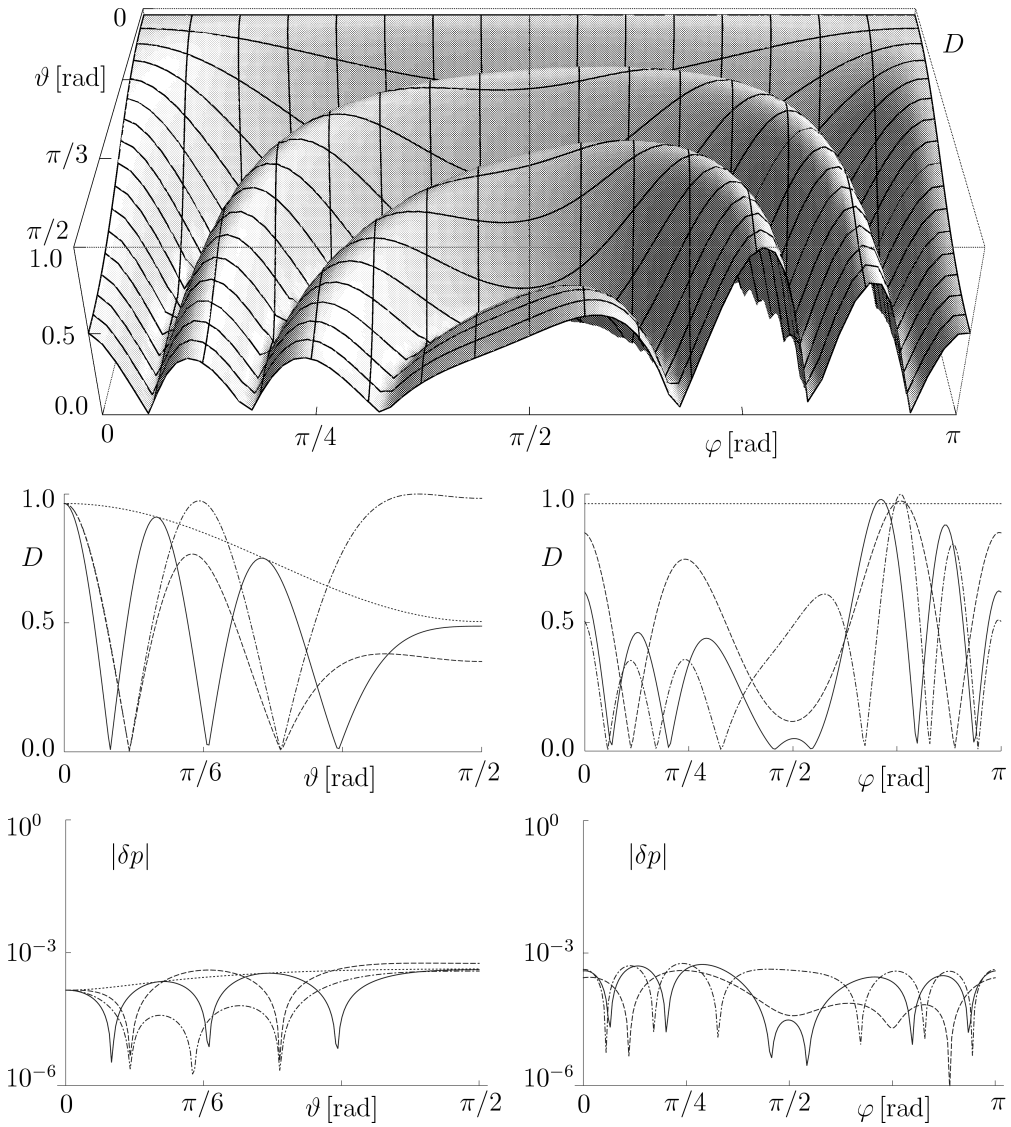

Fig. 3. The directivity factor D of vibrating membrane for the Dirac excitation, $\overline{r}_0 = a/2$, $\overline{\varphi}_0 = \pi/4$ and $L_{p,\mathrm{ref}} = 41.74$ [dB]. First row – perspective view, second row – intersections, third row – error estimation. Key: $\cdots\cdots$ $\varphi = 0, \pi$, $\vartheta = 0$; $- - -$ $\varphi = \pi/4$, $\vartheta = \pi/6$; ——— $\varphi = \pi/2$, $\vartheta = \pi/3$; $- \cdot - \cdot$ $\varphi = 3\pi/4$, $\vartheta = \pi/2$.

The normalized acoustic pressure amplitude

$$D = \frac{|p_N|}{p_{\mathrm{ref}}}, \qquad p_{\mathrm{ref}} = \max_{\vartheta,\varphi} |p_N| \tag{28}$$

has been presented in the figures where p_{ref} is the maximum of the acoustic pressure modulus within the region Ω. The index $N = 25$ denotes the limit

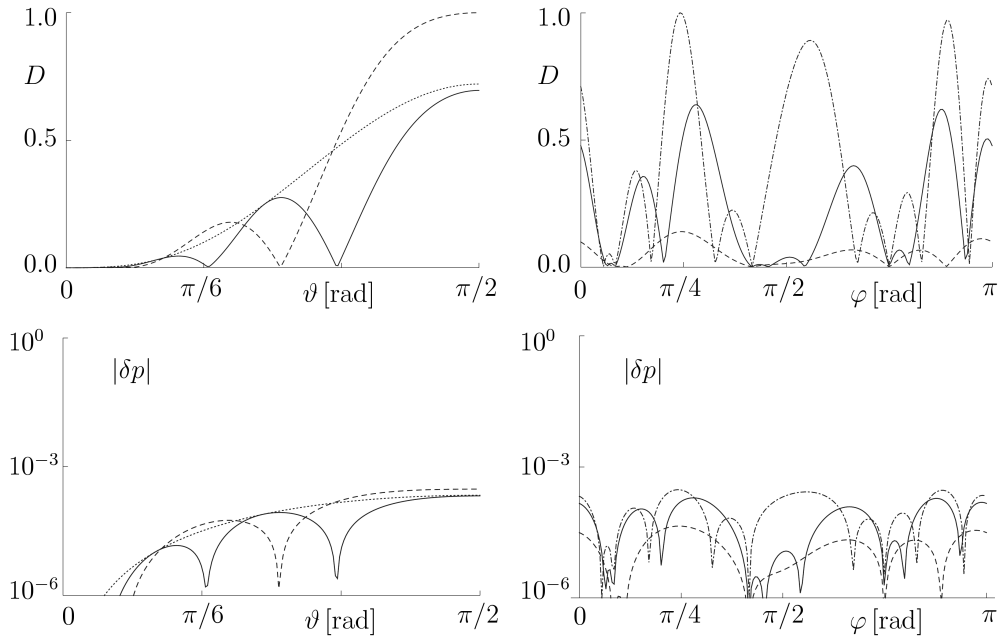

Fig. 4. The directivity factor D of vibrating membrane for the cosine excitation, $\overline{\varphi}_0 = \pi/4$, $M = 3$ and $L_{p,\mathrm{ref}} = 45.78$ [dB]. First row – intersections, second row – error estimation. Key: ····· $\varphi = 0, \pi$, $\vartheta = 0$; – – – $\varphi = \pi/4$, $\vartheta = \pi/6$; ——— $\varphi = \pi/2$, $\vartheta = \pi/3$; – · – · $\varphi = 3\pi/4$, $\vartheta = \pi/2$.

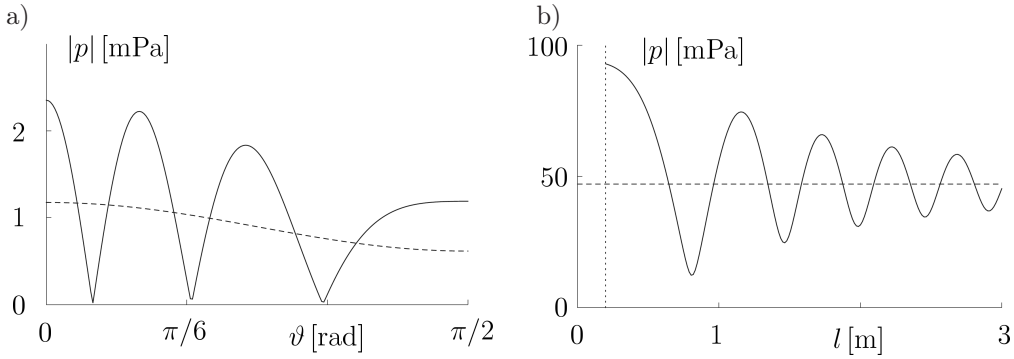

Fig. 5. The membrane's response $|p|$ for the Dirac excitation as the function of: a) ϑ for $L_{p,\mathrm{ref}} = 35.39$ [dB] – half-space and $L_{p,\mathrm{ref}} = 41.41$ [dB] – quarter-space; b) l for $r = 100$ [m], $L_{p,\mathrm{ref}} = 67.43$ [dB] – half-space and $r = 2.5$ [m], $L_{p,\mathrm{ref}} = 73.34$ [dB] – quarter-space. Key: ——— quarter-space, – – – half-space.

for the modenumbers m and n as in the previous subsection which means that $N^2 = 25^2$ initial modes have been used for numerical computations. The definition in Eq. (28) is similar to the directivity factor (Skudrzyk, 1971). The only difference is that the maximum acoustic pressure amplitude does not necessarily

appear at the source's main direction. The approximation of the acoustic pressure amplitude for any observation point $\mathbf{r} = (r, \vartheta, \varphi)$ can be obtained easily within the quarter-space by multiplying it by p_{ref} under the condition that $r \gg r_0$. The acoustic attenuation has been neglected during the numerical computations. However it can be included by using the values of the acoustic impedance while solving the algebraic equations system presented by Rdzanek, Rdzanek, and Szemela (2009) and computing the values of the coupling matrix $c^{(c)}_{m,n}$ and $c^{(s)}_{m,n}$ for a given excitation. The maximum of the acoustic pressure level has been computed using the following relation

$$L_{p,\text{ref}} = 10 \log_{10} \left(\frac{p^2_{\text{ref}}}{p^2_0} \right), \tag{29}$$

where $p_0 = 20$ [μPa] is the reference acoustic pressure. The approximation error has been defined as (cf. Eq. (27))

$$\delta p = \frac{p_{N=25} - p_{N=30}}{p_{\text{ref}}}, \tag{30}$$

where the meaning of N is identical as in Eq. (28).

In the case of the excitation f_1 the normalized acoustic pressure amplitude distribution has been obtained for a given value of the angle $\overline{\varphi}_0$ and presented in Fig. 3. The angle $\overline{\varphi}_0$ determines the numerical results introducing the asymmetricity clearly noticeable for $\overline{\varphi}_0 = \pi/4$ (the first two rows in Fig. 3). The results become similar to those valid for the vibrating circular piston for the values $\overline{\varphi}_0 = \pi/2, 3\pi/4$ (cf. Rdzanek, Szemela, and Pieczonka (2007) and the second row in Fig. 3). The main difference is that in the case of the membrane the localization of the acoustic pressure amplitude local extrema depends strongly on the angle φ for the growing values of the angle ϑ whereas it cannot be noticed for a vibrating piston. The approximation error does not exceed 1‰ within the entire range of the spatial variables ϑ and φ which means that the formulations for the acoustic pressure are useful in the entire region Ω in the far field (the third row in Fig. 3).

In the case of the circular membrane excitation by the function f_2 the straight nodal lines of the acoustic pressure distribution have been obtained for the fixed values of φ (the first row in Fig. 4). The nodal line of the acoustic pressure appears for $\overline{\varphi}_0 = \pi/4$, $M = 1$ and $\varphi \approx 3\pi/4$. If the number of the excitation nodal lines is increased to $M = 2$ then the nodal line of the acoustic pressure appears for $\varphi \approx \pi/2$ whereas if M is increased to the value of 3 then the three nodal lines of the acoustic pressure are obtained for $\varphi \approx \pi/10, 2\pi/5, 3\pi/4$. The estimated approximation error does not exceed 1‰ in the far field within the considered region Ω (the second row in Fig. 4).

The acoustic pressure amplitude radiated by a vibrating circular membrane has also been shown in Fig. 5. Figure 5a shows the quantity as the function of ϑ for $r = 100$ [m] and $\varphi = \pi/2$. The solid curve valid within the quarter-space is

much more directive and assume almost twice higher values at the local maxima than this valid within the half-space. Similar effect can be noted in the case of the radiation of a vibrating circular piston (Rdzanek *et al.*, 2007).

The acoustic pressure amplitude radiated by a vibrating circular membrane has been shown in Fig. 5b. The curve valid within the quarter-space begins from $l = a$ since the condition $l \geq a$ must be satisfied. Obviously, the curve valid in the half-space is not limited by this condition and does not depend on the variable l. Therefore, it begins in this figure from zero and does not vary with the change in l. It can be noted that the acoustic pressure amplitude is almost twice higher in the quarter-space than in the half-space on the main direction of the source, as expected. Several local maxima and nodes appear while changing variable l. This is caused by the superposition of the direct and reflected acoustic waves. The location of the maxima and the nodes depends on the distance l related to the wavelength of radiated waves, i.e. the distance measured in terms of the radiated wavelengths. The same situation appears for the vibrating circular piston (Rdzanek *et al.*, 2007). The value of 2.5 [m] has been selected for variable r in this figure to assure that the angle between the origins of the quarter-space and the source changes considerably with the change in l. This value is considerably smaller than in the previous figures. However, the ratio r/a is still much higher than unity as required in the far-field.

5. Concluding remarks

The problem of sound radiation by the vibrating circular membrane into the region of the quarter-space has been considered. As the result, the elementary equations have been found for the approximate value of the acoustic pressure amplitude. The equations enable numerical computations with the acoustic attenuation neglected as well as included. If the acoustic attenuation is to be included then the knowledge of the modal acoustic impedance presented by Rdzanek, Rdzanek, and Szemela (2009) is necessary. High accuracy of the numerical results has been achieved by conducting rigorous manipulations while analysing the approximate formulations. Significant differences in the acoustic pressure amplitude space distribution have been noticed for the excitations considered. It has been found that the differences result from the nature of the excitation, i.e. from the selection of the excitation as well as from choosing such the excitation parameter values as the number of nodal diameters M, the coordinates $\overline{r}_0, \overline{\varphi}_0$ and the amplitudes f_1 and f_2.

The values of the acoustic pressure amplitude of the vibrating circular piston located in the region of the quarter-space presented by Rdzanek, Szemela, and Pieczonka (2007) highly correspond with the results presented in this paper. The radiation of the vibrating circular piston and the radiation of the vibrat-

ing circular membrane show several similarities as well as significant differences depending strongly on the geometry of the excitation and its parameters.

The elementary equations presented in this paper enable determining the influence of the vertical wall presence on the acoustic pressure distribution including some different asymmetric excitations of the membrane. The investigations presented herein can be useful for predicting the acoustic pressure radiated into the regions bounded by the earth and some vertical walls often appearing in the urban and industrial environments. They can also be used to reduce the noise generated by the vibrating flat elements that can be modelled by the membrane excited asymmetrically. It is necessary to remember that the results presented are valid for small vibration velocities of the acoustic particles. The results presented herein are more useful than those presented by Rdzanek, Szemela, and Pieczonka (2007) since a deformable membrane is a better model for some real vibrating elements than a piston.

References

1. Arase E.M. (1964), *Mutual impedance of square and rectangular pistons in a rigid infinite baffle*, J. Acoust. Soc. Amer., **36**, 8, 1521–1525.
2. Batko W., Kozupa M. (2008), *Active vibration control of rectangular plate with piezoceramic elements*, Archives of Acoustics, **33**, 4, Supplement, 195–200.
3. Cieślik J., Pieczara J. (2008), *Precision analysis of vibration energy flux in angular connection of plates*, Archives of Acoustics, **33**, 4, Supplement, 201–206.
4. Dykas S., Wróblewski W., Rulik S., Chmielniak T. (2010), *Numerical method for modeling of acoustic waves propagation*, Archives of Acoustics, **35**, 1, 35–48.
5. Gołaś A., Filipek R. (2009), *Numerical simulation for the Bell directivity patterns determination*, Archives of Acoustics, **34**, 4, 415–427.
6. Gołaś A., Suder–Dębska K., Filipek R. (2010), *The influence of sound source directivity on acoustics parameters distribution in Kraków Opera House*, Acta Physica Polonica A, **118**, 1, 62–65.
7. Greenspan M. (1979), *Piston radiator: Some extensions of the theory*, J. Acoust. Soc. Amer., **65**, 608–621.
8. Hasheminejad S.M., Azarpeyvand M. (2004), *Sound radiation due to modal vibrations of a spherical source in an acoustic quarterspace*, Shock and Vibration, **11**, 625–635.
9. Kozień M., Wiciak J. (2009), *Choosing of optimal voltage amplitude of four pairs square piezoelectric elements for minimization of acoustic radiation of vibrating plate*, Acta Physica Polonica A, **116**, 3, 348–350.
10. Kozupa M., Wiciak J. (2010), *Active vibration control of rectangular plate with distributed piezoelements excited acoustically and mechanically*, Acta Physica Polonica A, **118**, 1, 95–98.
11. Krishnappa G., McDougall J.M. (1989), *Sound intensity distribution and energy flow in the nearfield of a clamped circular plate*, ASME Trans. J. Vib. Acoust. Stress Reliabil. Des., **111**, 465–471.

12. Le Clézio E., Delaunay T., Lam M., Feuillard G. (2008), *Piezoelectric material characterization by acoustic methods*, Archives of Acoustics, **33**, 4, 603–608.

13. Lee H., Singh R. (2005), *Acoustic radiation from out-of-plane modes of an annular disk using thin and thick plate theories*, Journal of Sound and Vibration, **282**, 313–339.

14. Leniowska L. (2008), *Influence of damping and fluid loading on the plate vibration control*, Archives of Acoustics, **33**, 4, 531–540.

15. Leniowska L. (2009), *Modelling and vibration control of planar systems by the use of piezoelectric actuators*, Archives of Acoustics, **34**, 4, 507–519.

16. Levine H., Leppington F.G. (1988), *A note on the acoustic power output of a circular plate*, Journal of Sound and Vibration, **121**, 2, 269–275.

17. Meirovitch L. (1967), *Analytical methods in vibrations*, MacMillan, New York.

18. Pawełczyk M. (2008), *Active noise control – a review of control-related problems*, Archives of Acoustics, **33**, 4, 509–520.

19. Piddubniak O., Piddubniak N. (2010), *Sound radiation from a roundabout*, Archives of Acoustics, **35**, 3, 437–456.

20. Rdzanek W. (1990), *Directional characteristic of a circular plate vibrating under the external pressure*, Archives of Acoustics, **15**, 1–2, 227–234.

21. Rdzanek W., Rdzanek W.P. (2006), *Green function for the problem of sound radiation by a circular sound source located near two-wall corner and three-wall corner*, Archives of Acoustics, **31**, 4, 99–106.

22. Rdzanek W.P., Szemela K. (2007), *Reduction of the sound power radiated by a two piston system located near the three-wall corner*, Archives of Acoustics, **32**, 2, 339–350.

23. Rdzanek W.P., Szemela K., Pieczonka D. (2007), *The sound pressure radiated into the far field by a circular piston located in the vicinity of the two-wall corner and the three-wall corner*, Archives of Acoustics, **32**, 4, 883–893.

24. Rdzanek W.P., Rdzanek W., Szemela K. (2009), *Acoustic power radiated into the quarter-space by a circular membrane with an asymmetric excitation*, Archives of Acoustics, **34**, 1, 75–94.

25. Rubinowicz A. (1971), *A sharpened formulation of Sommerfeld's radiation condition for Green's functions of the Helmholtz equation*, Reports on Mathematical Physics, **2**, 2, 93–98.

26. Shuyu L. (2000), *Acoustic field of flexural circular plates for air-coupled ultrasonic transducers*, Acta Acustica/Acustica, **86**, 388–391.

27. Skudrzyk E. (1971), *The Foundations of Acoustics*, Basic Mathematics & Basic Acoustics, Springer-Verlag, Wien, New York.

28. Stepanishen P.R. (1974), *Impulse response and radiation impedance of an annular piston*, J. Acoust. Soc. Amer., **56**, 2, 305–312.

29. Stepanishen P.R., Ebenezer D.D. (1992), *A joint wavenumber – time domain technique to determine the transient acoustic radiation loading on planar vibrators*, Journal of Sound and Vibration, **157**, 3, 451–465.

30. Svensson U.P. (2001), *Line integral model of transient radiation from planar pistons in baffles*, Acta Acustica/Acustica, **87**, 307–315.

31. Thompson Jr. W. (1971), *The computation of self- and mutual-radiation impedances for annular and elliptical pistons using Bouwkamp's integral*, Journal of Sound and Vibration, **17**, 2, 221–233.

32. Walerian E., Janczur R., Czechowicz M., Smyrnova Y. (2010), *Possible improvement of acoustical climate. Part I: Measurements and theoretical description*, Archives of Acoustics, **35**, 3, 395–420.

33. Walerian E., Janczur R., Czechowicz M., Smyrnova Y. (2010), *Possible improvement of acoustical climate. Part II: Possible solutions*, Archives of Acoustics, **35**, 4, 595–618.

34. Weyl H. (1919), *Ausbereitung elektromagnetischer wellen über einem ebenen leiter*, Annalen der Physik, 4te Folge, **60**, 481–500.

35. Weyna S. (2010), *Acoustic intensity imaging methods for in-situ wave propagation*, Archives of Acoustics, **35**, 2, 265–273.

36. Zou D., Crocker M.J. (2009), *Sound power radiated from rectangular plates*, Archives of Acoustics, **34**, 1, 25–39.

37. Zou D., Crocker M.J. (2009), *Response of a plate to PZT actuators*, Archives of Acoustics, **34**, 1, 13–23.